HAL open science

Modelling and simulation of coastal lagoons

Céline Acary-Robert, Loïc Dagnas, Antoine Rousseau

▶ **To cite this version:**

Céline Acary-Robert, Loïc Dagnas, Antoine Rousseau. Modelling and simulation of coastal lagoons. 2016. hal-01921054v1

HAL Id: hal-01921054

https://inria.hal.science/hal-01921054v1

Preprint submitted on 6 Jun 2016 (v1), last revised 13 Nov 2018 (v2)

HAL is a multi-disciplinary open access archive for the deposit and dissemination of scientific research documents, whether they are published or not. The documents may come from teaching and research institutions in France or abroad, or from public or private research centers.

L'archive ouverte pluridisciplinaire **HAL**, est destinée au dépôt et à la diffusion de documents scientifiques de niveau recherche, publiés ou non, émanant des établissements d'enseignement et de recherche français ou étrangers, des laboratoires publics ou privés.

Modelling and simulation of coastal lagoons

Application to the Tunqun lagoon, Chilean pacific coast

Céline Acary-Robert[b], Loïc Dagnas[c], Antoine Rousseau[a]

[a]*Inria and IMAG UMR 5159, Inria Chile, Av Apoquindo 2827, Las Condes, Santiago de Chile*
Antoine.Rousseau@inria.fr
[b]*LAMA, UMR 5127, Université Savoie Mont Blanc, Campus Scientifique 73376 Le Bourget du Lac*
Celine.Acary-Robert@univ-smb.fr
[c]*Inria Chile, Av Apoquindo 2827, Las Condes, Santiago de Chile*
loic.dagnas16@gmail.com

Abstract

The objective of this work is to provide a numerical model for the hydrodynamics of a lagoon located on the chilean coastline, characterized by an intermittent connection to the sea and a regular fresh water input coming from the Andes mountains. The model consists in a two-dimensional nonlinear shallow water system, including tracer equations for the time evolution of temperature and salinity. The water circulation in the lagoon accounts for external forcings such as water exchanges (with the atmosphere, rivers and sea), wind effects and external pumping. The paper includes a validation of the numerical method with respect to an analytical solution; numerical illustrations of involved geophysical processes and realistic simulation of typical scenarios of the Tunquén lagoon are provided.

Software availability. The software sources will be made available for download on a free accessible repository.

Keywords: Hydrodynamic modeling, Shallow water model, Finite volumes, Temperature and salinity simulations, Tunquen lagoon

1. Introduction

Numerous lagoon environments border the Chilean Pacific coast. These lagoons are often simultaneously connected with ocean, rivers and groundwater sources. In addition, these ressources are mostly located in dry and possibly arid environments, making them very fragile and sensitive to changes. From the ecological point of view, these lagoons are of interest because they fulfill fundamental ecological functions such as hydrological regimes regulation; they also provide shelters for specific flora and fauna, specially for water birds. Moreover, these lagoons play an important micro- and macro-climatic role due to the evapotranspiration which allows to regulate the local level of humidity and rain.
In this work, we are interested in a particular site: the Tunquén lagoon. Located closed to large Chilean cities (Valparaiso at 45 km and Santiago at 130 km) but with a low anthropic activity, it is one of the few places in the region that preserves a high biodiversity surrounding the Casablanca's stream mouth. Tunquén is known to be of great value for the landscape and the environment. Useful informations can be found in the geographic study [1]: it defines precisely the lagoon context and its fragile ecosystem.
The lagoon is located on the coastline and is sometimes (mostly during winters) be connected to the ocean; rivers and groundwater sources supply the lagoon with fresh water coming from the nearby mountains. As for many shallow water ressources, Tunquén is very much subject to wind constraints. Finally, water can be pumped out of the lagoon for watering purposes by a local resort.

Tunquén is sensitive to the desertification and global level climate changes. This area, located near large cities, also undergoes an important real-estate pressure which leads to major modifications of the landscape

(the decrease in the vegetation has been observed as stated in [1]) and a risk of contamination due also to increasing tourism activities.

Finally, let us recall that this lagoon is classified as "Sanctuario de la Naturaleza" by the Chilean government. This classification means, according to [2, Section 31], that this site permits the study of geology, palaeontology, zoology, botanic or ecology, or hosts natural formations interesting for science or the state. This underlines the particular ecological interest of the area.
For all these reasons, people are interested in numerical simulations of such a lagoon, which allow to determine the importance of various parameters such as meteorological conditions, variations of different water supplies, etc.

Coastal lagoons such as Tunquén are complex systems in which freshwater flowing from inland rivers meets the sea, creating a combination of fresh and salt-water (subject to seasonal changes) and resulting in fragile and complex ecosystems that are often significantly influenced by human activities. To the best of our knowledge, no hydrodynamical study has ever been performed in Tunquén, as it has been done for numerous european lagoons[1] such as Cabras (Italy, see [3]), Venice (Italy, see [4]) or Thau (France, see [5] and [6]). In all these studies, incompressible nonlinear shallow water equations have been used to simulate the water motion, with additional equations for passive tracers (salt and temperature): this is for exemple the framework of *Shyfem*[2], a finite element model for shallow water hydrodynamics.

In this work we propose a complete viscous shallow water model, including wind and rain-evaporation terms, together with passive tracers such as salinity (c.f. [3]) or temperature. Contrary to Shyfem, we choose a numerical resolution based on the *finite volume* method, implemented in the open source C++ library *OpenFoam*[3] and precisely described in [7]. In the following, the hydrodynamical model (including forcing processes) is described in Section 2. Section 3 introduces numerical aspects: the numerical toolbox is first described in Section 3.1, then we use academic configurations (squared box, analytical bathymetry and forcings) to validate the numerical model versus an analytical solution (see Section 3.2) and comment on basic geophysical processes (see Section 3.3). We end this article with realistic simulations over the Tunquén lagoon (see Section 4). Perturbations of the hydrological system by slight modifications of external forces are also analyzed.

2. Lagoon modelling

In this section, we start from the traditional Navier-Stokes equations and recall the series of approximations and assumptions that lead to the nonlinear shallow water model (NSW) that will be used in the sequel. Then we introduce equations for tracers such as salinity and temperature.

2.1. Shallow water hydrodynamics

2.1.1. Notations

We consider a bounded and regular domain $\Omega \subset \mathbb{R}^2$, typically a lagoon surface, with boundary $\partial\Omega$. The bathymetry and the water height are respectively described by the functions $h_0 : \Omega \to \mathbb{R}$ and $h : \Omega \times \mathbb{R} \to \mathbb{R}$ such as the water volume is the three-dimensional set:

$$\Omega_3 = \{(x, y, z) \in \mathbb{R}^3, s.t.(x, y) \in \Omega,\ h_0(x, y) \leq z \leq H(x, y, t)\},$$

where the total height H is given by $H(t, x, y) = h(t, x, y) + h_0(x, y)$ (see Figure (1)). These notations are also used by the C++ library OpenFoam that we have been using for numerical simulations (see Section 3).

[1]The Water Framework Directive 2015 has fostered many studies in Europe.
[2]See `https://sites.google.com/site/shyfem/home`.
[3]See `http://www.openfoam.com/`.

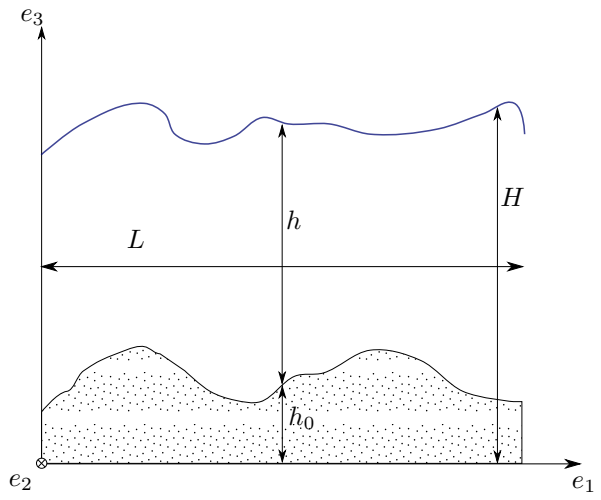

Figure 1: Notations for the NSW equations

2.1.2. Navier-Stokes equations

The traditional Navier-Stokes equations (without rotational terms) for incompressible flows write:

$$\rho\partial_t u + \nabla\cdot(\rho u^T u) = \nabla\cdot(\sigma - pI_d) - \rho g e_3, \tag{1a}$$

$$\nabla\cdot u = 0. \tag{1b}$$

The explicit form for the tensor σ is given by:

$$\sigma = \mu(\nabla u + {}^T\nabla u).$$

We supplement these equations with boundary conditions traducing respectively the free surface kinematic condition at the top of Ω_3, together with no penetration and Navier conditions at the bottom:

$$\sigma_T\cdot n_{|z=H} = 0, \tag{2a}$$

$$u\cdot e_{3|z=h_0} = 0, \tag{2b}$$

$$(\kappa u - \sigma\cdot n)_{|z=h_0} = 0, \text{with } \sigma_T = \sigma - pI_d. \tag{2c}$$

2.1.3. Integration of Shallow Water equations

We now proceed to a series of approximations that will take us from the complete Navier-Stokes equations (1) to the NSW model.

Approximation 1 (Constant density). *In the sequel, we assume that the water density of the lagoon is constant. This approximation is more restrictive than the usual Boussinesq approximation (which consists in assuming a constant density everywhere but in the buoyancy term occuring in the (vertical) momentum equation* (1a)*).*

With this approximation, setting $\rho\equiv 1$, our equations read:

$$\partial_t u + \nabla\cdot(u^T u) = \nabla\cdot(\sigma - pI_d) - g e_3, \tag{3a}$$

$$\nabla\cdot u = 0. \tag{3b}$$

In the case where the 3D domain Ω_3 is such that its aspect ratio H/L is small enough, we consider a second approximation:

Approximation 2 (Hydrostatic). *Provided that the horizontal scale is large compared to the vertical scale, the vertical pressure gradient may be given as the product of density times the gravitational acceleration.*

Accounting for these two aproximations, the fundamental equations simplify as the so-called primitive equations of the ocean (see for example [8] or [9]) that get rid of the vertical acceleration and replace the third momentum equation by the so-called hydrostatic approximation:

$$\frac{\partial p}{\partial z} = -\rho\, g. \tag{4}$$

We need a third hypothesis (see [10]) to finally obtain the so-called shallow water equations, namely:

Approximation 3 (Vertical averaging). *The horizontal velocity is close to its vertically averaged value, which can be obtained when $\mu = O(\varepsilon)$ (see [10]).*

Finally, we obtain the following NSW equations:

$$\partial_t(h\overline{U}) + \nabla\cdot(h\overline{U}^T\overline{U}) + gh\nabla(h+h_0) + \frac{\kappa}{1+\frac{\kappa h}{3\mu}}\overline{U} - 4\mu\nabla(h\nabla\overline{U}) = 0, \tag{5a}$$

$$\partial_t(h) + \nabla\cdot(h\overline{U}) = 0. \tag{5b}$$

2.2. Equations for tracers

Generic transport-diffusion equations. As we previously did for the NSW model, we integrate the classical three dimensional transport diffusion equation of a passive marker r between h_0 and H. Assuming this marker constant along the vertical axis, it leads to the following 2D transport-diffusion equation for r:

$$\partial_t r + \overline{U}\cdot\nabla r - D_r\Delta r = S_r, \tag{6}$$

where D_r is the diffusion coefficient associated to r, S_r is an integrated source term.

Temperature. Assuming that the temperature is a passive marker constant along the vertical axis, we have:

$$\partial_t T + \overline{U}\cdot\nabla T - D_T\Delta T = S_T, \tag{7}$$

where D_T is the diffusion coefficient, S_T is a forcing term traducing the temperature variations during days and seasons.

Salinity. The salinity behaviour is modeled by a similar transport diffusion equation:

$$\partial_t s + \overline{U}\cdot\nabla s - D_s\Delta s = 0, \tag{8}$$

where s is assumed constant along the vertical axis, and D_s is the diffusion coefficient.

2.3. External forces

We now exhibit all the hydrodynamical external forcing processes.

2.3.1. Wind

The wind is an external forcing τ in the momentum equation (5) such as:

$$\partial_t(h\overline{U}) + \nabla\cdot(h\overline{U}^T\overline{U}) + gh\nabla(h+h_0) + \frac{\kappa}{1+\frac{\kappa h}{3\mu}}\overline{U} - 4\mu\nabla(h\nabla\overline{U}) = \tau,$$

with τ the surface tension define according to [3] by:

$$\tau = \frac{\rho_a}{\rho_e}C_d \parallel \overline{U} \parallel \overline{U}, \tag{9}$$

where ρ_e is the water density considered to be constant equal to 1, ρ_a is the air density and C_d is called the training or dragging coefficient. We will use for numerical simulations the expression of C_d given in [11]:

$$C_d = 10^{-3}(0.63 + 0.066 \parallel \overline{U} \parallel). \tag{10}$$

2.3.2. Evaporation and rain

We chose to model the evaporation-rain effect by a source term $\eta : \Omega \times \mathbb{R} \to \mathbb{R}$ in the NSW conservation equation (5). We rewrite then (5) as:

$$\partial_t(h) + \nabla \cdot (h\overline{U}) = \eta, \tag{11}$$

where η corresponds to the temporal variation of water height due to rain and evaporation. As rain and evaporation impact also the salinity, (8) has to be modified as follows:

$$\partial_t s + \overline{U} \cdot \nabla s - D\Delta s + \frac{\eta s}{h} = 0, \tag{12}$$

where the new term $\eta s/h$ can be obtained thanks to a balance of salt in an elementary water column. As a matter of fact, rain implies salt dilution whereas evaporation implies salt concentration.

2.4. The complete model

Including all tracers and external forces, the lagoon system can be rewritten as:

$$\partial_t(h\overline{U}) + \nabla \cdot (h\overline{U}^T\overline{U}) + gh\nabla(h + h_0) + \frac{\kappa}{1 + \frac{\kappa h}{3\mu}}\overline{U} - 4\mu\nabla \cdot (h\nabla\overline{U}) = \tau, \tag{13a}$$

$$\partial_t(h) + \nabla \cdot (h\overline{U}) = \eta, \tag{13b}$$

$$\partial_t s + \overline{U} \cdot \nabla s - D\Delta s + \frac{\eta s}{h} = 0, \tag{13c}$$

$$\partial_t T + \overline{U} \cdot \nabla T - D_T\Delta T = S_T. \tag{13d}$$

This model has to be supplemented with appropriate initial and boundary conditions which depend on the lagoon configuration. Typically, the boundary conditions for passive markers will be Dirichlet conditions for inflow and Neumann conditions for outflow. The boundary conditions for h will be Neumann whereas the boundary conditions for hU will be Dirichlet for inflow or outflow, and a slip condition for the sides of the domain.

3. Numerical model: framework and validation

3.1. OpenFoam library

So as to simulate the lagoons dynamics, we used the opensource finite volume C++ library OpenFoam®(Open Field Operation and Manipulation). Distributed since 2004, this software is able to solve numerically classical physical problems using the Finite Volume Method (FVM). OpenFoam is born from a London Imperial College project, the basis of the project is the Thesis [7], and an important and frequently updated documentation can be found in the following helpful OpenFoam toolboxes[4].

OpenFoam gives access to generic solvers for numerous classical problems: thermal diffusion, 3D Navier-Stokes equations, shallow water and many others, using various numerical schemes. The NSW solver furnished by OpenFoam, called *shallowWaterFoam*, used a numerical scheme mixing SIMPLE and PISO. PIMPLE is an OpenFoam algorithm which tie SIMPLE and PISO algorithm: it is a predictor-corrector algorithm including multiple correction steps and relaxation.

[4]See the following repositories:

- The unofficial OpenFOAM wiki, `http://www.openfoamwiki.net/`,
- CFD Direct: OpenFOAM Training, Development and Support, `http://www.cfd.direct`,
- The openFoam Foundation and CFD toolbox, `http://www.openfoam.org`.

We extended the *shallowWaterFoam* solver in a new one called *shallowWaterLagoonFoam* which could take into account salinity and temperature transport-diffusion, wind effect and rain-evaporation source terms, as in the model (13) above.

3.2. Analytical solution and numerical validation

Provided that equations (13c)-(13d) are simple transport-diffusion equations that can be decoupled from equations (13a) and (13b), we focus on the validation the hydrodynamics and now identify an analytical solution of:

$$\partial_t(h\overline{U}) + \nabla\cdot(h\overline{U}^T\overline{U}) + gh\nabla(h+h_0) + \frac{\kappa}{1+\frac{\kappa h}{3\mu}}\overline{U} - 4\mu\nabla\cdot(h\nabla\overline{U}) = \tau, \tag{14}$$

$$\partial_t(h) + \nabla\cdot(h\overline{U}) = \eta. \tag{15}$$

3.2.1. Analytical solution

We consider the computational domain $\Omega = (0,L)\times(0,l)\times(h_0,h)$, where the bathymetry h_0^* is plotted in Figure 2 and defined with the following analytical formula:

$$h_0^* = \alpha\, sin^2(4\pi\frac{x}{L}). \tag{16}$$

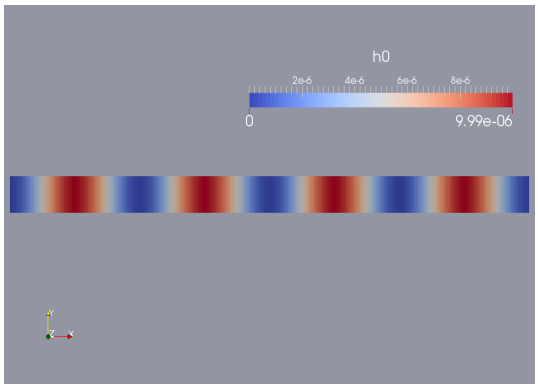

Figure 2: Bathymetry h_0, with $\alpha = 10^{-5}$.

Let $f(x,y) = 1+\lambda\, sin^2(\pi\frac{x}{L})\, sin^2(\pi\frac{y}{l})$. We choose external forcing terms $\tau^* = (\tau_x^*, \tau_y^*)$ and η^* as follows:

$$\begin{aligned}\tau_x^*(x,y) &= 2\,\lambda\,\frac{\pi}{L}sin(\frac{\pi x}{L})\,cos(\frac{\pi x}{L})\,sin^2(\frac{\pi y}{l}) \\ &\quad + g\,f(x,y)\left(2\,\lambda\,\frac{\pi}{L}\,sin(\frac{\pi x}{L})\,cos(\frac{\pi x}{L})\,sin^2(\frac{\pi y}{l}) + \frac{8\pi\alpha}{L}\,sin(\frac{4\pi x}{L})\,cos(\frac{4\pi x}{L})\right) \\ &\quad + \frac{\kappa}{1+\frac{\kappa f(x,y)}{3\mu}},\end{aligned} \tag{17}$$

$$\tau_y^*(x,y) = 2\,\lambda\,\frac{\pi g}{l}\,f(x,y)sin^2(\frac{\pi x}{L})\,sin(\frac{\pi y}{l})\,cos(\frac{\pi y}{l}), \tag{18}$$

$$\eta^*(x,y) = 2\,\lambda\frac{\pi}{L}\,sin(\frac{\pi x}{L})\,cos(\frac{\pi x}{L})\,sin^2(\frac{\pi y}{l}). \tag{19}$$

One can then easily check that

$$h^*(t,x,y) = f(x,y) = 1+\lambda\, sin^2(\pi\frac{x}{L})\, sin^2(\pi\frac{y}{l}), \tag{20}$$

$$U^*(t,x,y) = (u^*, v^*) = (1,0), \tag{21}$$

is a steady solution of equations (14)-(15) with the following boundary conditions:

	x=0	x=L	y=0	y=l
hU	$(1,0,0)$	$\partial_x(hU)=0$	$\partial_y(hU_x)=0,\ (hU)_y=0$	$\partial_y(hU_x)=0,\ (hU)_y=0$
h	1	1	1	1

3.2.2. Numerical experiments

We use OpenFoam to compute a numerical solution of equations (14)-(15) with the above boundary conditions. The initia data are $h=1$, $hU=(1,0)$ and we run the model from $t=0$ to $t=50$s. Then we compute the following errors:

- space map of the relative error at $t=50s$:

$$Err_{hU}(x,y)=\frac{\|hU-h^*U^*\|}{\|h^*U^*\|}, Err_h(x,y)=\frac{|h-h^*|}{|h^*|}.$$

- time variation of the RMS error:

$$Err_{hU,2}=\left(\frac{1}{V}\int_0^L\int_0^l\frac{\|hU-h^*U^*\|^2}{\|h^*U^*\|^2}\right)^{1/2}, Err_{h,2}=\left(\frac{1}{V}\int_0^L\int_0^l\frac{|h-h^*|^2}{|h^*|^2}\right)^{1/2}.$$

Figures 3 and 4 provide slots of the errors for one single set of numerical parameters ($l=2$m, $L=30$m, $\alpha=10^{-5}$, $\lambda=10^{-5}$, $\Delta t=0.05$s, $\Delta x=0.15$m and $\Delta y=0.05$m.). These slots illustrate the capability of the numerical model to solve the NSW equations with non trivial forcings and geometry.

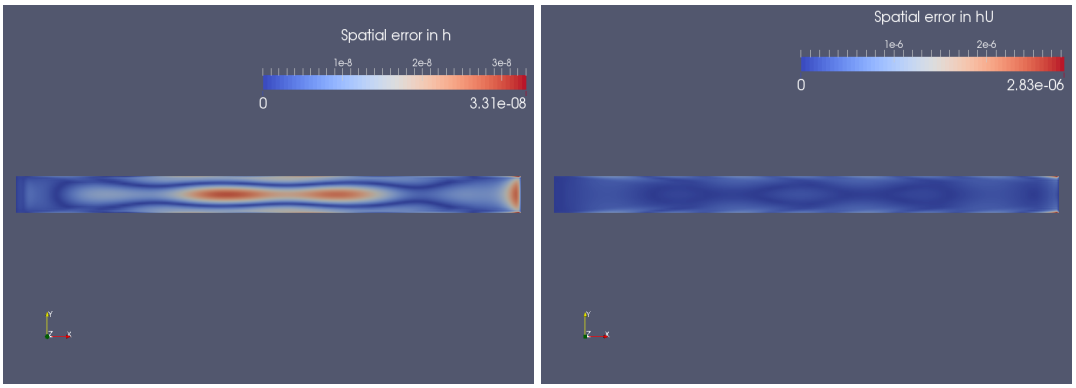

Figure 3: Space map of the error at $t=50s$ for the water height h (left) and outflow hU (right).

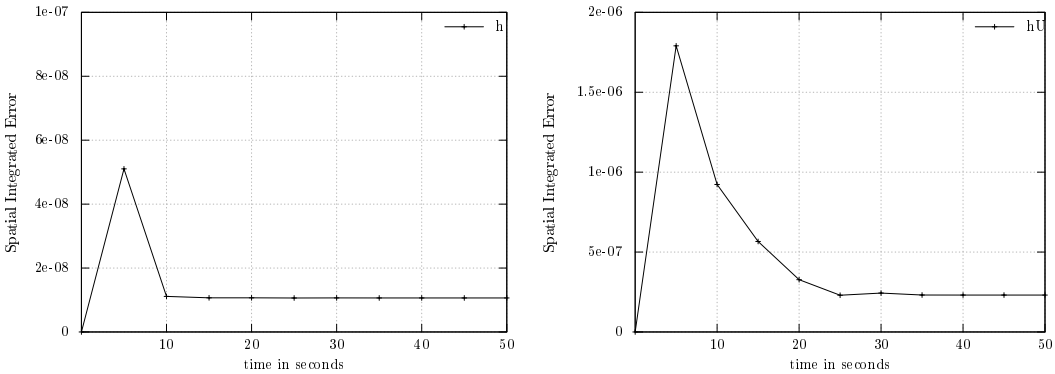

Figure 4: Time variation of the RMS error for the water height h (left) and outflow hU (right).

Remark 1. *We provide in Table 1 a comparison of the error with different values for the bathymetry amplitude α (λ being constant in this set of simulations). Similarly, we present the same error in Table 2 but this time α remains constant and we allow the wave amplitude λ to vary.*
We recall that both parameters α and λ are expected to be small in shallow water regime: higher α would require non-hydrostatic modeling, whereas higher λ would necessitate the addition of dispersive terms.

$\lambda = 10^{-5}$	$\alpha = 10^{-5}$	$\alpha = 10^{-4}$	$\alpha = 10^{-3}$	$\alpha = 10^{-2}$
Error in hU	$2.3.10^{-7}$	$2.3.10^{-6}$	$2.3.10^{-5}$	$2.3.10^{-4}$
Error in h	$1.1.10^{-8}$	$4.9.10^{-8}$	$4.8.10^{-7}$	$4.8.10^{-5}$

Table 1: Final RMS error (at $t = 50$s) with several values for the bathymetry oscillation amplitude α.

$\alpha = 10^{-5}$	$\lambda = 10^{-5}$	$\lambda = 10^{-4}$	$\lambda = 10^{-3}$	$\lambda = 10^{-2}$
Error in hU	$2.4.10^{-7}$	$8.4.10^{-7}$	$8.3.10^{-6}$	$8.4.10^{-5}$
Error in h	$1.1.10^{-8}$	$9.5.10^{-8}$	$9.5.10^{-7}$	$9.4.10^{-6}$

Table 2: Final RMS error (at $t = 50$s) with several values for the wave oscillation amplitude λ.

3.3. Illustration of single geophysical processes

Before using our new solver on the Tunquén lagoon we perform some additional validations and illustrate each physical process on a simple test case. The test case we use is based on the *squareBump* test case furnished by OpenFoam. The principle of this test case is summarized in Figure 5. It is an inflow outflow problem, the boundary inflow and outflow hU are fixed, initially there is no velocity and the water salinity is constant.

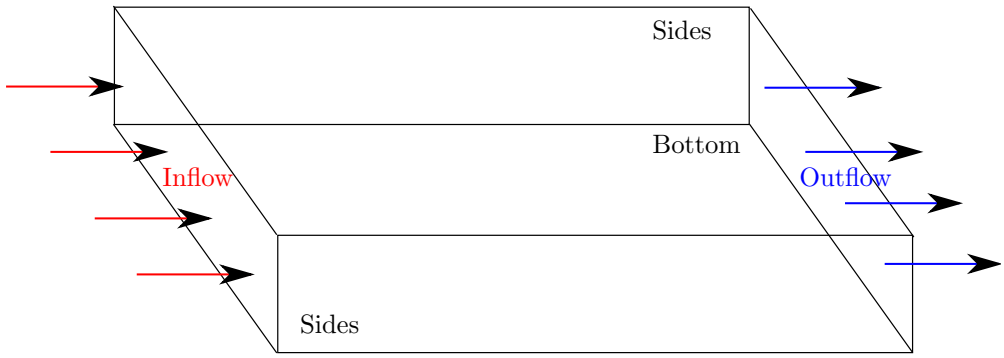

Figure 5: squareBump test case (3D illustration but 2D model).

Salinity with constant inflow outflow

The simplest case is the following: we observe the salinity with an inflow and outflow fixed to $hU = 10^{-4}\mathrm{m}^2.\mathrm{s}^{-1}$. The boundary conditions for salinity are Dirichlet conditions on the left side of the box and Neumann for all other sides. Results are given in Figure 6 and show a predictable behaviour of transport-diffusion of salt along the the whole domain.

Salinity propagation

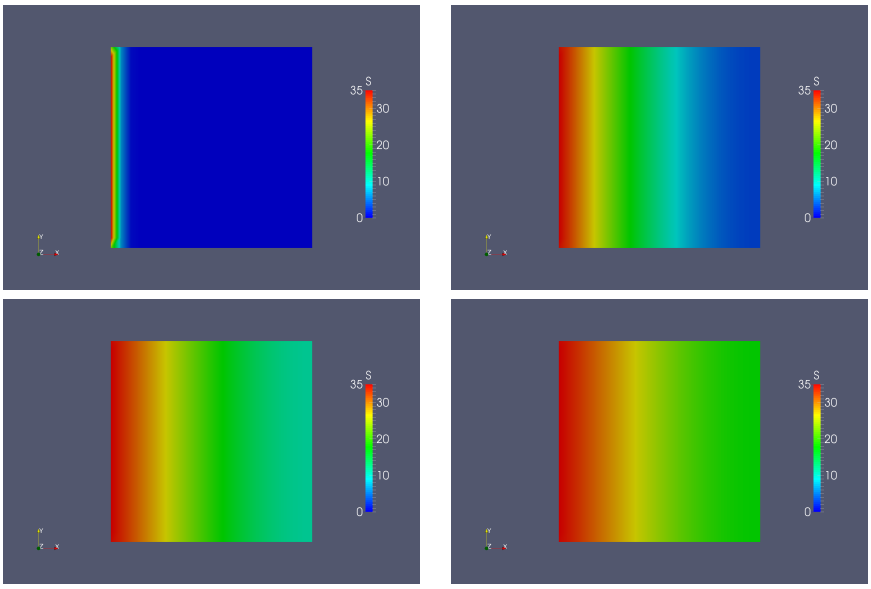

Figure 6: From left to right, salinity propagation at $t = 1, 200, 400, 600$s.

Evaporation without inflow outflow

An illustration of the salinity variation only due to evaporation (without inflow or outflow) is given in Figure 7. For this case, the water is initially at rest in the squared box and the evaporation is imposed in a small square centered in the domain. We can see that the salinity is increasing in the evaporation zone. Initially the zone of salinity variation is squared, but as expected it rapidly spreads to a circular shape.

Salinity and evaporation

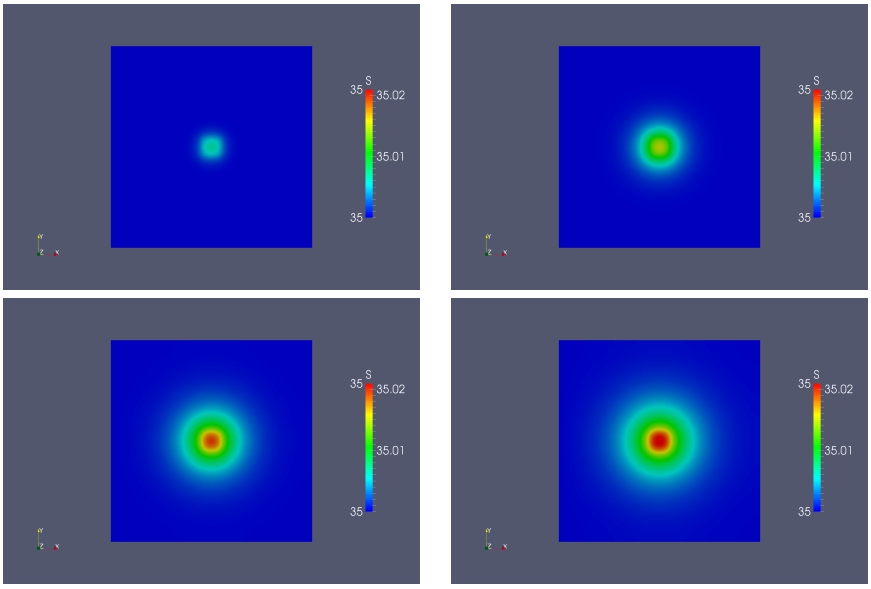

Figure 7: From left to right, salinity propagation at time $t = 25, 150, 350, 500$s with $\eta = 10^{-}5$ m.s^{-1}.

Wind effect without inflow outflow

In this experiment, we simulate a constant wind from the left to the right of the domain. The water is initially at rest in the squared box and there is no inflow outflow during the experiment (wall boundary condition). We can see in Figure 8 that this source term is creating motion in the water domain with a quite important magnitude. Since there is no outflow, the water motion is firstly going from left to right (wind direction) and then recirculate along the closed boundaries.

Wind effect

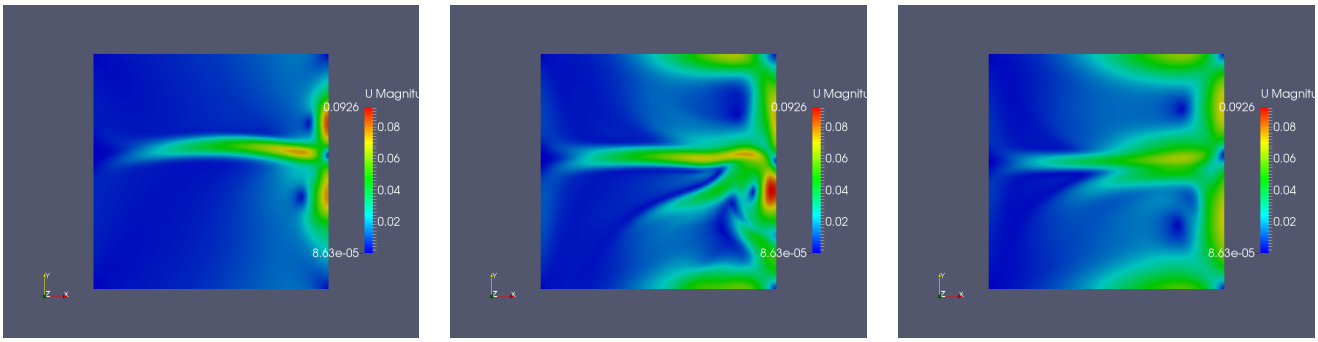

Figure 8: From left to right, water velocity magnitude in a closed box at $t = 350, 450, 550$s with $U_{wind} = 10$ m.s^{-1} along the horizontal direction (left-right).

Temperature with constant inflow outflow and parabolic bathymetry

An illustration of the temperature variation is given in Figure 10, with a parabolic bathymetry (c.f. Figure 9). The boundary condition for temperature is fixed to $T = 15^o$C on the left side of the domain and homogeneous Neumann conditions (thermal insulation) on the other sides. The initial condition is set to $T = 20^o$C everywhere.

In addition to the diffusion process that smoothes temperature gradients, one can see in Figure 10 that the

temperature fronts are transported with the velocity, which itself strongly depend on the bathymetry (see Figure 9).

Parabolic bathymetry

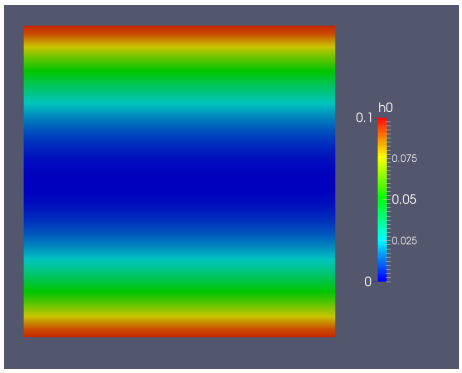

Figure 9: Parabolic bathymetry h_0 in the square bump.

Temperature and parabolic bathymetry

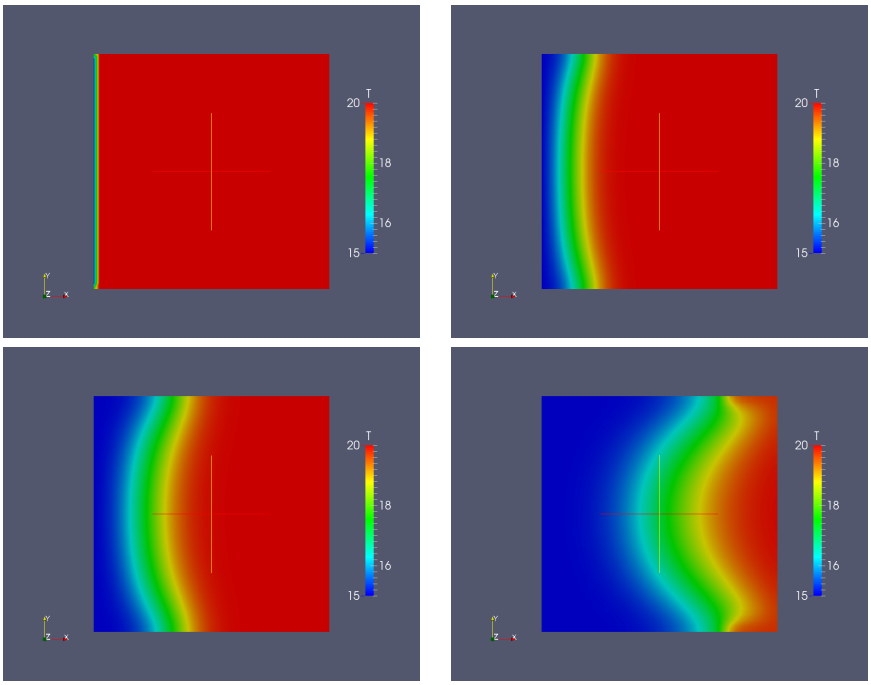

Figure 10: From left to right, temperature at $t = 1, 200, 400, 1000$s

4. A realistic application: the Tunquén lagoon

The objective of this Section is to use the numerical model (introduced in Section 2 and validated in Section 3) in the configuration of the Tunquén lagoon located in the the center of Chile. This lagoon presents some characteristic features of a coastal lagoon: river, intermittent connexion with the sea, dry continental climate, etc. We also recall that with respect to data, the shape of the lagoon is available thanks to satellite

images but neither the bathymetry nor the mean salinity, temperature and volume of the lagoon have been measured. One of the objectives of such a work is to encourage Tunquén residents and decision makers to collect such data. Considering rain and wind, we only have a description of a typical wind day and some sparse measures of rain. Despite this lack of real data, we will show that our model is able to deal with the different processes and is ready to integrate efficiently real data. We present here some simulation results concerning different atmospheric *scenarii*. After reaching a stable state which will be detailed later, we study the influence of wind, rain, evaporation and connection with the sea on the flow in the lagoon. We also analyse the nonlinear effects of the bathymetry and resulting modifications of the water flow in the lagoon.

4.1. Physical characteristics of the Tunquén lagoon

4.1.1. Shape and resulting mesh

We drew the shape of the lagoon thanks to a satellite view, and then, given points on the hull, we generate the digital shape so as to mesh the domain. The meshing has been performed with the free software *gmsh*. We obtain our meshed lagoon ready for OpenFoam as we can see in Figure (11).

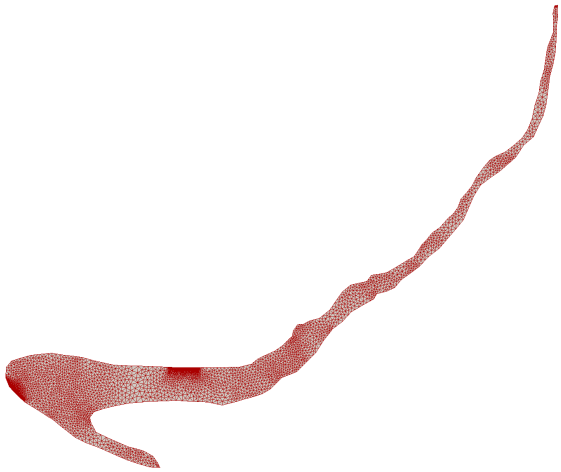

Figure 11: Tunquén lagoon meshed by gmsh. The mesh is refined near areas of interest.

4.1.2. Boudary conditions and forcings

Beside the fact that the mesh is 2D, we can impose the shape of the bed in the lagoon. The influence of the shape of the bed will be also discussed in the next part. The Tunquén lagoon is connected to a river in the north-east part and intermittently connected to the sea in the south-west part (typically connected in winter). A pump is also located in the northern coast. These connections are summarized in Figure (12). Finally, the surface is submitted to rain, evaporation and wind.

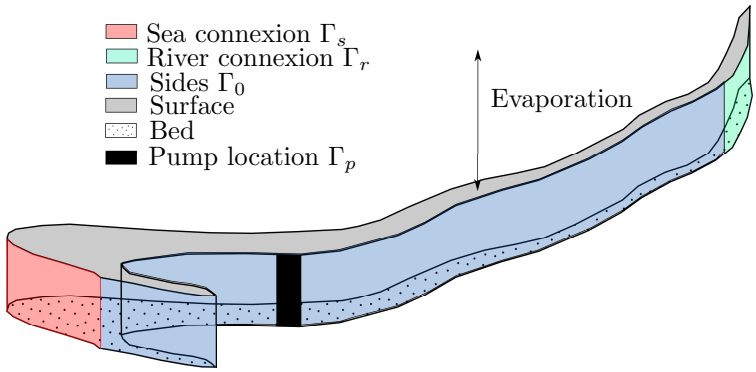

Figure 12: Tunquén lagoon boundaries (3D illustration but 2D model)

We now describe the system inflows and outflows. All these connections will be written as boundary conditions on the water height h and discharge hU. The boundary condition on h will always be homogeneous Neumann *i.e.*

$$\nabla h \cdot \underline{n}_{j\Gamma} = 0, \quad \text{with } \Gamma = \Gamma_0 \cup \Gamma_p \cup \Gamma_s \cup \Gamma_r \tag{22}$$

River connection. For the river connection, the discharge hU is very dependant to the season and the climate. That is why we decided to model the river inflow as a sinusoidal function which reaches it maximum in the middle of spring (melting snow) and autumn (rain), and a minimum in the middle of summer (drought) and winter (glaciers):

$$\forall (x,y) \in \Gamma_r,\ \forall t > 0, \begin{cases} (hU)(x,y,t) \cdot \underline{n} & = (\underline{U_r} + U_{r,1} \sin(2\pi f_r t))\alpha_r(x,y) \\ (hU)(x,y,t) \cdot \underline{t} & = 0, \end{cases} \tag{23}$$

with $\underline{n}$ and $\underline{t}$ the normal and tangent vectors of Γ_r, $\frac{1}{f_r} = 6$ months, $\underline{U_r}$ average value of hU such as there is no outflow and $U_{r,1}$ the amplitude of the sinusoidal function.

So as to avoid singularity close to the extremity of Γ_r, we decide to use a Poiseuille profile for the velocity on Γ_r:

$$\alpha_r(x,y) = 1 - \frac{r(x,y)^2}{R^2}, \tag{24}$$

where $r(x,y)$ can be easily find thanks to the points A, B, I_{AB} et M defined in Figure (13).

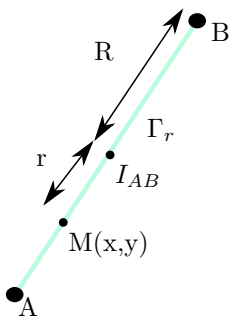

Figure 13: Poiseuille profile

Pump connection. For the pumping area, same kind of considerations lead to the following choice:

$$\forall (x,y) \in \Gamma_p,\ \forall t > 0, \begin{cases} (hU)(x,y,t) \cdot \underline{n} & = \underline{U_p}\alpha_p(x,y) \\ (hU)(x,y,t) \cdot \underline{t} & = 0, \end{cases} \tag{25}$$

with $\underline{n}$ and $\underline{t}$ the normal and tangent vector of Γ_p, $\underline{U_p} > 0$ average value of hU to impose such as there is a null inflow, α_p is defined in a same way that we did in (24).

Sea connection. To model the connection between the sea and the lagoon, we consider two oscillating phenomena: the tide (low frequency behaviour) and the waves (high frequency behaviour). Then, our modelling choices can be written as:

$$\forall (x,y) \in \Gamma_s,\ \forall t > 0, \begin{cases} (hU)(x,y,t) \cdot \underline{n} & = (\underline{U_s} + U_{s,1}\cos(2\pi f_m t) + U_{s,2}\cos(2\pi f_w t))\alpha_s(x,y) \\ (hU)(x,y,t) \cdot \underline{t} & = 0, \end{cases} \tag{26}$$

with $\underline{n}$ and $\underline{t}$ the normal and tangent vector of Γ_s, f_m and f_w tidal and waves frequencies, $\underline{U_s}$ the average value of the debit, $U_{s,1}$ and $U_{s,2}$ the amplitudes of both sinusoidal functions. α_s is defined in a same way that we did in (24).

Evaporation-rain connection. We want to chose an expression for the rain-evaporation function η which can depend on time (season, climate) and space (shadow). It can be written on Ω as:

$$\eta(x,y,t) = \eta_0(x,y) + \eta_1(x,y)\sin(2\pi f_r t). \tag{27}$$

4.2. Numerical results

The main objective of this part is to study the influence of the different parameters such as bathymetry, atmospheric conditions and connections. In order to get a stable state to initiate the test cases for the atmospheric *scenarii*, we firstly run a full year of lagoon dynamics without the sea connection (six first months) and then with connection (six last months, see Figure (15) for an illustration in the case of salinity).

4.2.1. Reference state

The sea connection is modelled by successive twelve hours tides, the inflow from the river is a six months sinusoid, and the pump outflow is constant. Finally, in this first simulation, the lagoon is isolated from the atmosphere.

The main objective of this first year of modelling the circulation of the water in the lagoon is to reach a "stationnary" state, far from the beginning of the initial flow. For this first year, two simulations are performed to compare a flat bathymetry (the initial height of water is constant everywhere) with a smooth step in the middle of the domain as described in Figure (14) after one year.

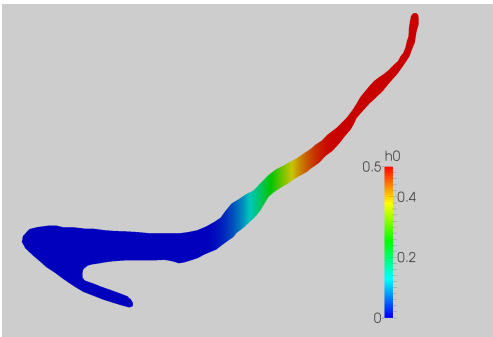

Figure 14: Assumed bathymetry for the Tunquén Lagoon (smoothed step).

For the last 6 months, some fresh water is entering the lagoon at the river connection and some salted water at the sea connection.

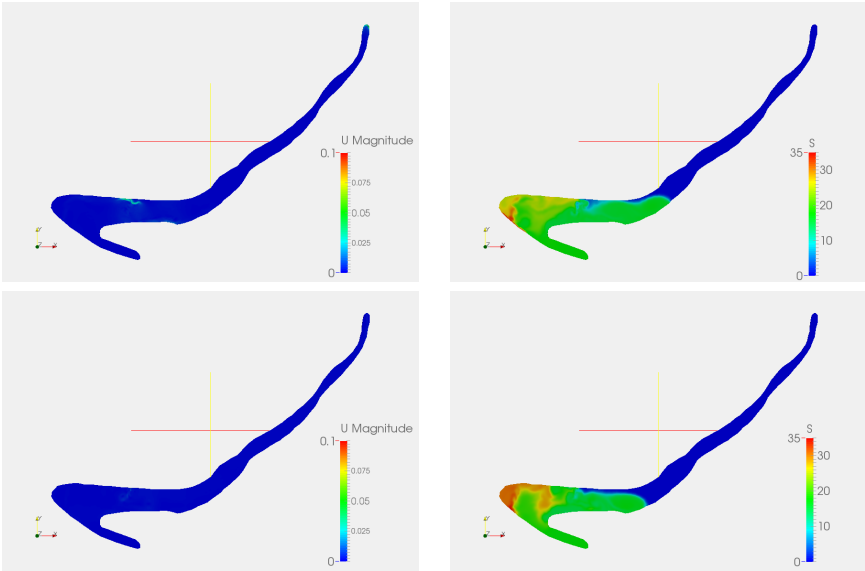

Figure 15: Stable state after one year. Salinity and velocity for flat bathymetry (upper) and smooth step (lower).

As expected, we observe in both cases that the salinity is decreasing in the northern part of the lagoon thanks to the river water inflow, and increasing (after the six first months) in the southern part thanks to the sea water inflow. Due to the difference of the shapes of the bathymetry, the resulting state is different, both for the magnitude of the velocity and the salinity.

4.2.2. Typical atmospheric perturbations

Before studying wind or tide effects on the hydrodynamics, let us say a word about two simple simulations for which - for the sake of brevity and clarity - we do not show any figure:

- **Rain** We apply a realistic quantity of rain of 10 mm during a day (c.f. [1]): twelve hours with rain and twelve hours without rain. As expected, the results show a variation of 10 mm of the water height and a dilution of salt.

- **Day-night temperature variation** We apply a sinusoidal variation of temperature of the atmosphere (24 hours variations from the minimum value of 10^oC for the night to the maximum value 20^oC for the day). As a consequence, the water temperature oscullates at the same frequency.

A typical wind scenario

In the work of [1], we can find the description of a typical wind scenario which consists in a main orientation (East-West) with a change of direction during the day and the night. For instance, we apply to the lagoon twelve hours of West-East wind (15 m.s^{-1} during the day) and then twelve hours of East-West wind (15 m.s^{-1} during the night) to study its influence on the lagoon main water flow. As detailed in [12], the dominant effects governing the main flow of such lagoons is the interaction between the bathymetry and strong winds. In this work, we have run two main simulations: a flat bathymetry and a smooth step to compare the effect of the wind on the flow regarding to the shape of the bed. The results are shown in Figure (16).

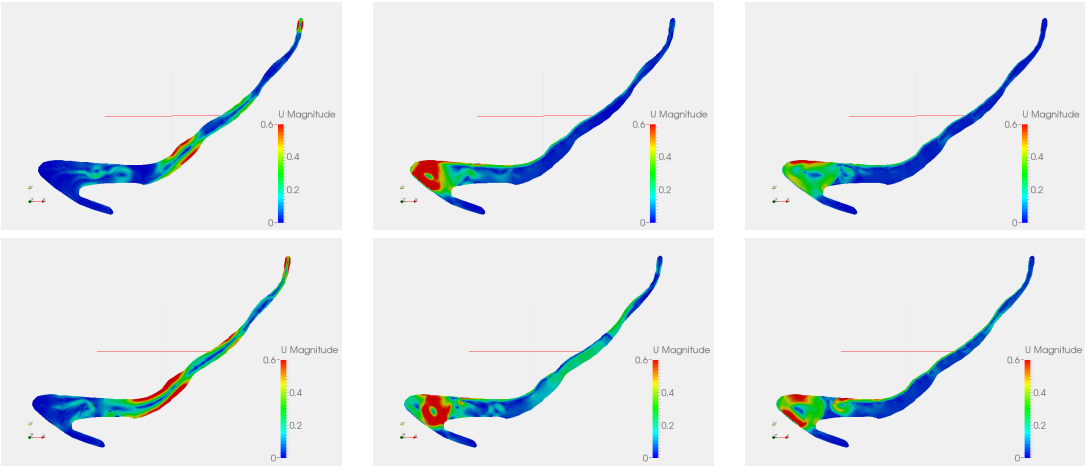

Figure 16: Magnitude of velocity at time 11 hours 40 minutes (left), 13 hours (center) and 23 hours and 20 minutes (right), for flat bathymetry (upper) and smooth step (lower).

As expected the wind has an important impact on the water velocity, and then it orientates the water flows and the transport of any marker. Since the wind direction is horizontal, we can see an increase of water velocity where the domain shrinks and turns.

The comparison between the result with the flat bathymetry and the smooth step underlines the nonlinear effects of the bathymetry in such processes. As we can see in Figure (16), in the smooth step case, the velocity of the flow is increased near the step in the first part of the scenario (when the wind goes from West to East). Moreover, the flow along the northern coast, when the height is lower, is increased in magnitude, generating a swirl where the bed is deepening. This effect is significantly lower in the flat case.

Large tide effect

In this experiment, we used the smooth step bathymetry for our study. We want to analyze the influence of a larger tide entering the lagoon during two hours. After two days without sea connection, we model a constant water inflow from the sea to the lagoon during two hours, like a very large tide which would reach the lagoon during two hours. Then we wait four more days without connection to sea the salt diffusion. In Figure (17), we give the salinity representation.

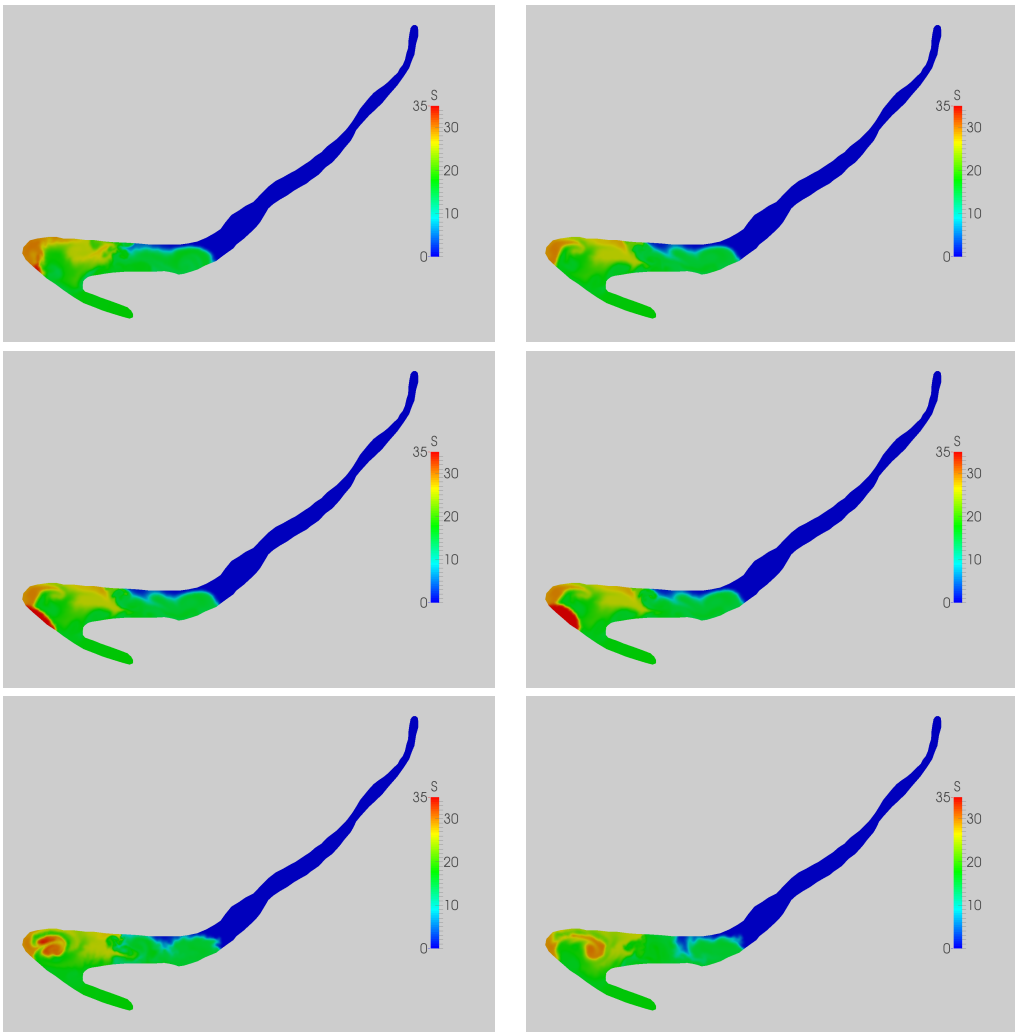

Figure 17: Salinity for a large tide, from left to right and top to bottom, day 0 and day 2 without sea connection, hour 1 and hour 2 of large tide, day 1 and day 2 after the end of the large tide

The transport-diffusion behaviour is satisfying and convincing, we can easily imagine the motion of an other passive marker in the water, a pollutant for instance. In the third and the fourth sub-figures of Figure (17), we can see the important inflow of salted water, and in the fifth and sixth sub-figures the propagation in the domain of a salted plume after the end of sea connection.

Acknowledgments

The authors are grateful for the support from Inria Chile and the research LabEx NUMEV.

References

[1] F. O. Carrasco, C. G. Rossel, Diagnóstico territorial en espacios naturales, estudio de caso: Sitio prioritario humedal de tunquén. región de valparaíso. in spanich only, Ph.D. thesis, Pontificia Universidad Catolica de Valparaiso (2008).

[2] Ministerio de Educación, Gobierno de Chile, Ley n°17.288 de monumentos nacionales y normas relacionadas, Consejo de Monumentos Nacionales.

[3] C. Ferrarin, G. Umgiesser, Hydrodynamic modeling of a coastal lagoon: The cabras lagoon in sardinia, italy, Ecological Modelling 188 (24) (2005) 340 – 357.

[4] C. Ferrarin, G. Umgiesser, A. Cucco, T.-W. Hsu, A. Roland, C. Amos, Development and validation of a finite element morphological model for shallow water basins, Coastal Engineering 55 (9) (2008) 716 – 731.
[5] A. Ruopp, P. Daus, A. Ruprecht, S. RiedelBauch, Fonctionnement hydrodynamique du bassin de thau. validation écologique dun modèle numerique de circulation, Oceanologica Acta 12 (1) (1989) 37–46.
[6] E. Frénod, A. Rousseau, Paralic confinement: Models and simulations, Acta Applicandae Mathematicae 123 (1) (2013) 1–19.
[7] H. Jasak, Error analysis and estimation for the finite volume method with applications to fluid flows, Ph.D. thesis, Imperial College, London (1996).
[8] P. Azérad, F. Guillén, Mathematical justification of the hydrostatic approximation in the primitive equations of geophysical fluid dynamics, SIAM J. Math Anal. 33 (2001) 847–859.
[9] M. Petcu, R. Temam, M. Ziane, Mathematical problems for the primitive equations with viscosity, in: P. G. Ciarlet (Ed.), Handb. Numer. Anal., Elsevier, New York, 2008.
[10] J.-F. Gerbeau, B. Perthame, Derivation of viscous saint-venant system for laminar shallow water; numerical validation, Discrete and Continuous Dynamical Systems - Series B 1 (1) (2001) 89–102.
[11] S. Smith, E. Banke, Variation of the sea surface drag coefficient with wind speed, Quarterly Journal of The Royal Meteorological Society 101 (1975) 665–673.
[12] E. ALekseenko, B. Sukhinov, R. Kortaba, D. Fougere, Nonlinear hydrodynamics in a mediterranean lagoon, Nonlin. Processes Geophys. (2013) 189–198.